COBEM 2023 27TH INTERNATIONAL CONGRESS OF MECHANICAL ENGENEERING

ABCM Brazilian Society of Mechanical Sciences and Engineering
27th ABCM International Congress of Mechanical Engineering
December 04-08, 2023, Florianópolis-SC, Brazil

COB-2023-0701
COMPARATIVE STUDY OF THE RESIDUAL STRESS INDUCED BY LASER SURFACE HARDENING OF AISI 1020 AND AISI 4130 STEELS

Ana Sofia Seibel Pinto Andreão
Gabriela Rocha Profilo
Rogério Lima Mota de Oliveira
Sheila Medeiros de Carvalho
Olga Liskevych

Federal University of Espirito Santo, Vitoria – Brazil

e-mail: anasofia_andreao@hotmail.com, gabrielaprof@hotmail.com, rogerio.mota@eb.mil.br, sheila.m.carvalho@ufes.br, olga.liskevych@ufes.br

Abstract. *Laser hardening is an advantageous option among the variety of surface treatments of materials due to its flexibility, accuracy, good control of heat input in fusion and heat-affected zones, limited grain growth during heating and low distortion. Moreover, this procedure allows to increase the hardness of the surface region of the treated material without compromising the ductile properties of the substrate. As a consequence of temperature gradients and microstructural changes during heating and cooling cycles in hardened materials, residual stress can develop influencing resulting material properties and service exploitation. The purpose of this work was to investigate changes in the residual stress state after surface laser hardening of AISI 1020 and AISI 4130 steels, as well as its consequences for the properties of the aforementioned materials. To accomplish this objective, the magnitude and nature of the residual longitudinal and transversal stresses in the reference and laser processed samples were measured using the ESPI-based hole-drilling method. Afterwards, the local residual stress distribution was compared to the phase transformation occurred during hardening and microhardness of the processed areas. The results obtained in this study show that the materials exhibit different performances when subjected to laser hardening treatment under identical process conditions. Both materials showed martensite formation in the surface area, but only the AISI 4130 steel sample exhibited compressive stress induced during the hardening process. Meanwhile, tensile stress induction was observed in the AISI 1020 steel sample throughout the analyzed depth. The same effect was reported for both longitudinal and transversal components. Regarding the microhardness results, the AISI 1020 steel showed an increase of almost 87% when superficially hardened, while the AISI 4130 steel presented only an increase of approximately 61%. Therefore, in accordance with the results of this study, it was possible to conclude that despite the same process parameters during the treatment, the AISI 4130 steel presents a more effective application of laser surface hardening when compared to the AISI 1020 sample.*

Keywords: *laser hardening, residual stress, AISI 1020, AISI 4130, microhardness*

1. INTRODUCTION

The utilization of lasers in surface heat treatments encompasses a broad range of applications, among which laser hardening stands out as a prominent technique. Laser hardening has gained considerable attention as a surface modification technique, offering exceptional improvements in the hardness, wear resistance, and fatigue strength of steels. There are numerous advantages to using this method, including controlled thermal penetration and controlled distortion, ease of automation, controlled thermal profile, and absence of chemical contamination. No cooling liquid is required for the quenching of the component. The low energy input results in minimal distortion. Additionally, there are cost savings in production since post-treatment machining operations are not necessary.

By employing a high-intensity laser beam to selectively heat the surface of a material followed by rapid cooling, laser hardening induces a desirable microstructural transformation, predominantly forming martensite, which imparts enhanced mechanical properties. However, this rapid thermal cycle and localized heating introduce significant thermal gradients and thermal stresses, ultimately leading to the development of residual stress within the material.

Residual stress is an intrinsic phenomenon that arises in materials as a consequence of various manufacturing processes, including laser hardening, and is defined as stress that remains in the component when all external loads and/or temperature gradients are removed (Lu, 1996). It plays a pivotal role in determining the mechanical properties, performance, and reliability of engineering components. According to Totten et al. (2002), residual stresses can bring either detrimental or beneficial effects to components, and this outcome depends on several factors such as material

condition, stress nature (whether it is tensile or compressive), magnitude and stability of residual stresses, mechanical load and environmental conditions. Therefore, the performance of a material used in a component is influenced by the presence of residual stresses, where their distribution and magnitude play a significant role in product design and manufacturing processes.

Understanding and characterizing residual stress in laser-hardened steels is of paramount importance for optimizing the design, fabrication, and service life of these materials in a wide range of industrial applications. In recent years, extensive research efforts have been devoted to investigating the characteristics, distribution, and evolution of the residual stress in laser-hardened steels. Numerous factors, including laser parameters, material composition, initial microstructure, and cooling rates, exert influence over the magnitude and distribution of residual stress. A comprehensive understanding of these factors is critical for optimizing laser hardening processes and minimizing the risk of material failure due to stress-induced cracking, distortion, or reduced fatigue life. Thus, Gao et al. (2017) conducted a comprehensive investigation of the residual stress and mechanical properties of laser hardened AISI 4340 steel, offering valuable insights into the relationship between the laser hardening parameters and the resultant stress development. Huang et al. (2015) examined the influence of laser hardening on residual stress and mechanical properties of 30CrMnSiA steel, contributing to our understanding of material-specific responses to laser hardening. Sun et al. (2016) explored the effects of laser power and scanning speed on residual stress and mechanical properties of selective laser melted 316L stainless steel, thereby providing valuable insights into the influence of process parameters on stress generation. Ahmad et al. (2021) performed a detailed analysis of the residual stress in laser-hardened AISI 4140 steel using the deep-hole drilling method, further enriching our understanding of the stress distribution in laser hardened steels. Marimuthu et al. (2017) investigated the effect of laser hardening on the residual stress distribution in AISI 304 stainless steel, yielding significant insights into the stress profiles of laser hardened stainless steels.

In its turn, this paper also aims to provide a comprehensive analysis of the residual stress in laser-hardened steels, with a particular focus on two commonly utilized steels: AISI 1020 and AISI 4130. The objective was to explore the effects of laser hardening on the residual stress profiles of these materials discarding the influence of previous manufacturing processes and shed light on the underlying mechanisms governing the development of residual stress in hardened steels depending on their chemical composition and microstructure. Overall, the present study highlights the importance of understanding the residual stress in laser-hardened steels and the need for careful consideration of process parameters and material selection in order to optimize the performance and reliability of these materials in industrial applications. By continuing to advance our understanding of residual stress in laser-hardened steels, we can pave the way for further improvements in the design, fabrication, and performance of these materials in the years to come.

2. MATERIALS AND METHODS

For the purpose of this study, 3 mm thick samples of AISI 1020 and AISI 4130 were used as base materials, and their respective chemical compositions are provided in Tabs. 1 and 2, respectively.

Table 1. Chemical composition (%) of the AISI 1020 samples.

C	Si	P	S	Cr	Ni	Mn
0.200	0.220	0.015	0.028	0.055	0.18	0.660

Table 2. Chemical composition (%) of the AISI 4130 samples.

C	Si	P	S	Cu	Cr	Ni	Mo	W
0.280	0.290	0.800	0.007	0.010	1.000	0.150	0.250	0.004
V	**Nb**	**Co**	**Al**	**Sn**	**As**	**Sb**	**N**	**H_2**
0.026	0.003	0.01	0.022	0.008	0.006	0.0026	0.004	0.00014

2.1. Specimen preparing

Laser surface hardening of both studied materials was carried out using a 2-kW continuous wave fiber laser produced by IPG Co, according to the procedure arrangement shown in Fig. 1. The focal length was set as 160 mm with a minimum spot diameter of 100 μm. Since the actual beam radius ω(Z) depends on the position of the sample surface with respect to the focal plane, its value can be defined as given by Eq. (1):

$$\omega(Z) = \omega_0 \left[1 + \left(\frac{M^2 \lambda . Z}{\pi . \omega_0^2}\right)^2\right]^{1/2} \quad (1)$$

where [Z] is the distance from the focal plane, [ω_0] is the minimum beam radius, [M] is the beam quality factor and [λ] is the laser wavelength. In this study, [Z] was used as 12:2 mm, ω_0 and λ were equal to 50 μm and 1:080 μm, respectively. The laser beam quality [M] was measured as 9, Z = −4 mm and ω = 0:25mm.

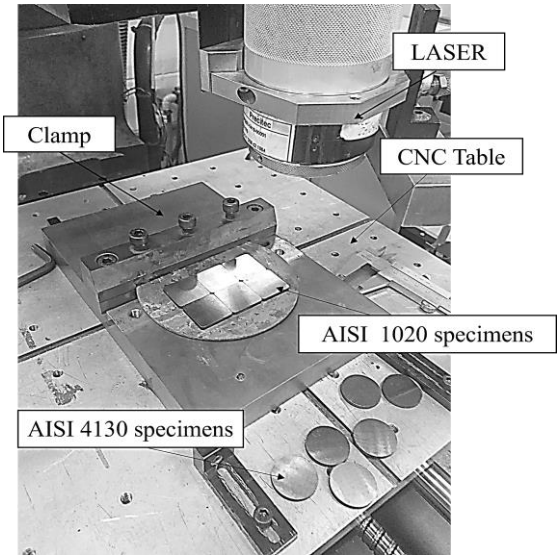

Figure 1. Laser surface hardening arrangement of AISI 1020 and AISI 4130 specimens.

Sample movement was performed using a CNC table that could move at a constant velocity from 1 to 160 mm/s and could be programmed in any direction in an area of 430 × 500 mm^2. The Z-axis is also computer-controlled with a 1 μm step resolution and is used to change the focal distance [Z] in Eq. (1). For surface processing in this study, the laser beam was moved in a square zigzag pattern with partial superposition between each track. Since the lateral shift between each laser track was 0.5 mm, and as the beam diameter was estimated by Eq. (1) as 0.5 mm, the theoretical superposition between each laser track was zero. Ten-second delay was fixed between one track and another to avoid overheating. After optimizing the process parameters, the scanning speed was fixed at 10 mm/s and the laser beam power was set as 150 W. When the heat input (HI), i.e., the power/speed ratio, was higher than 15 J/mm, surface damage was severe. On the other hand, when HI < 15 J/mm, the surface seemed unchanged.

The samples were surface-processed under ambient conditions, that is, without protective shielding gas. To assess the effect of the surface condition, the samples were C-coated (coated with a graphite layer) after grinding. The thickness of the graphite layer was approximately 10μm, as evaluated by the scotch method; however, this value could change due to the manual spraying procedure.

After the aforementioned surface processing, destructive and non-destructive testing were carried out using the samples shown in Fig. 2 and Fig. 3 for the AISI 1020 and AISI 4130, respectively. Samples numbered as 1 for each material were used as the reference samples, where the residual stress, microhardness, and metallography were analyzed in as-received condition in order to avoid the previous manufacturing processes influence on the analysis conducted in this study. Samples numbered as 2 for both the studied materials were used for cross-sectional analysis of metallography and samples numbered as 3 were used for residual stress evaluation.

The purpose of metallography was to visualize the microstructure of the reference and hardened samples, as well as phase-changing observation and depth of the heat treatment evaluation. It was performed using standard cutting, grinding and polishing methods, followed by chemical etching with Nital 2% (2% nitric acid in ethanol). By employing an optical microscope and commercial image treatment software, it was possible to discern the dimensions of the heat-affected zones of the treated samples. On its turn, the microhardness was measured using Vickers pyramid of MHT3 equipment produced by Anton Paar. Indentations were performed using a 200 mN load, starting with 40 μm from the surface depth and using 100 μm intervals between measurements reaching a final depth of 1340 μm.

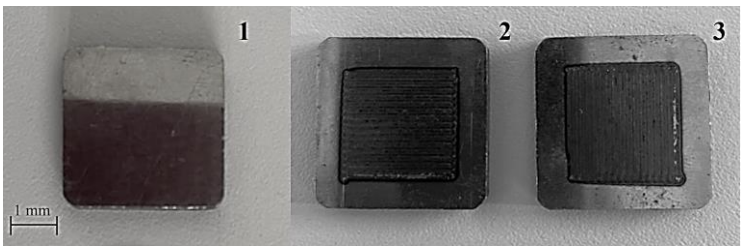

Figure 2. AISI 1020 studied specimens: (1) reference sample (2) and (3) laser-hardened samples.

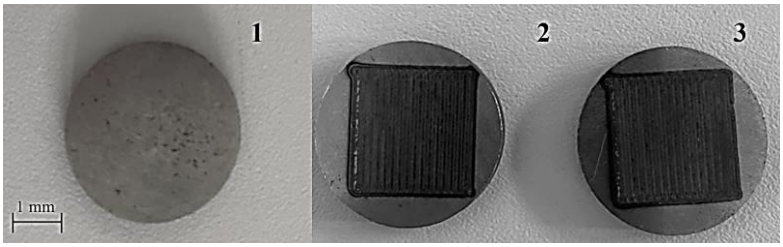

Figure 3. AISI 4130 studied specimens: (1) reference sample (2) and (3) laser-hardened samples

2.2. Residual stress measurement

In this study, residual stress measurements were performed using the equipment shown in the Fig. 4, which consists of a camara for image capture, a drilling tool, a sample fixture device and a laser beam with all its known properties. This beam is divided into two parts: the first is launched on the sample and reflected to the camera, while the second (referred to as the reference beam) passes through a piezoelectric phase change system and is subsequently directed to the same optical device. When a hole is drilled in the sample and the stress induced by thermal processing is relieved by local deformation, the light beam reflected from the surface of the sample changes its characteristics. When compared to the reference beam, the reflected beam exhibits a phase shift which leads to the new grain pattern (pixels) in the recorded camera images. From the difference in pixel arrangement before and after drilling, i.e., before and after stress relief, a speckle pattern is obtained (see Fig. 5). Subsequently, the spackle patterns are processed as digital interferograms with an equipment algorithm, as demonstrated by Steinzig and Ponslet (2003), in order to obtain the local surface displacements caused by the machining of the sample and corresponding residual stress present in the material before drilling.

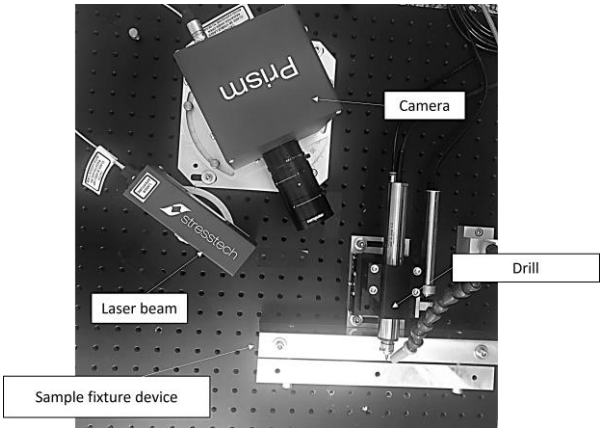

Figure 4. Equipment arrangement for residual stress measurement using the hole-drilling method combined with the EPSI technique.

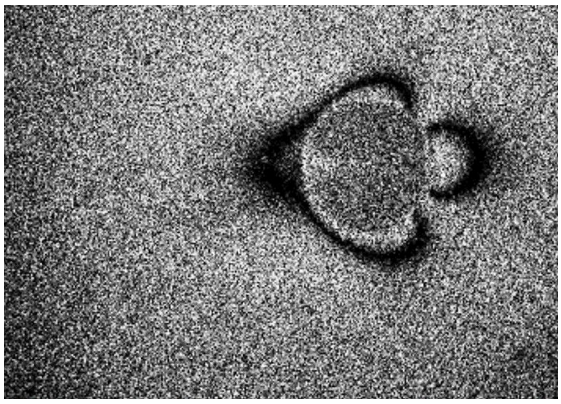

Figure 5. Speckle pattern caused by residual stress relief during hole opening.

The equipment described aforehand was calibrated using a standard four-point bending device and strip specimen with known properties (ASTM, 2000), demonstrating a 5.8% mean measurement error associated with the measurement uncertainties of the plunge indicator, elasticity modulus variation of material, as well as, with the error sources of the equipment itself. More details are provided by Liskevych et al. (2022). Both for calibration purposes and residual stress evaluation in hardened samples, series of measurements were carried out drilling 0.8 mm diameter hole at a rotational speed of 25000 rpm and 0.05 mm/s feed rate reaching the maximum hole depth of 0.4 mm (Upshaw et al., 2011; Barile et al., 20014). During machining, at each of 0.05 mm drilling increment, images were captured as shown in Fig. 6 with interferometry pattern shifts due to the changes occurring in the stress state of the material. After interferogram processing, the values of the measured stress in the longitudinal and transversal directions, were provided for further analysis, along with the rate of poor pixels detected on the captured images.

3. RESULTS AND DISCUSSION

Cross-section micrography of the reference samples, i.e., those that were not laser-hardened, can be observed on the Fig. 7. The microstructures of both materials are represented by a ferritic phase (light gray color) and a pearlite composite (dark gray color), however, the pearlitic structure of AISI4130 is way more prominent.

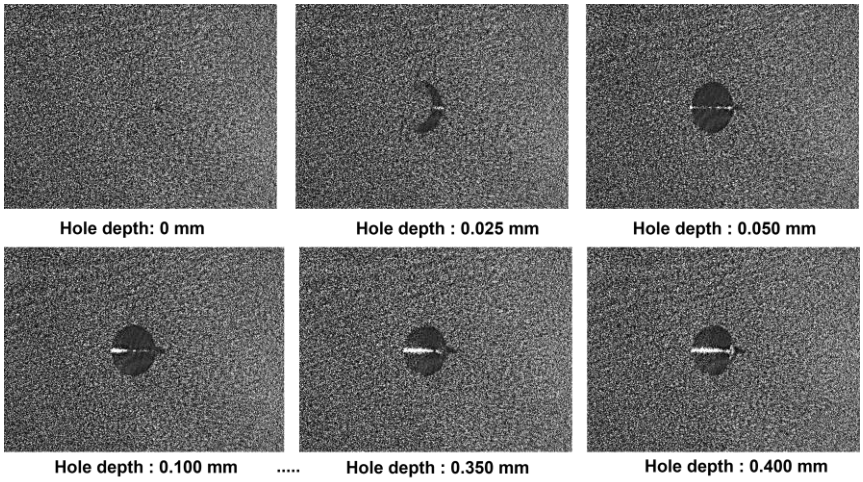

Figure 6. The image quality pattern at each drilling increment processed in order to obtain residual stress values.

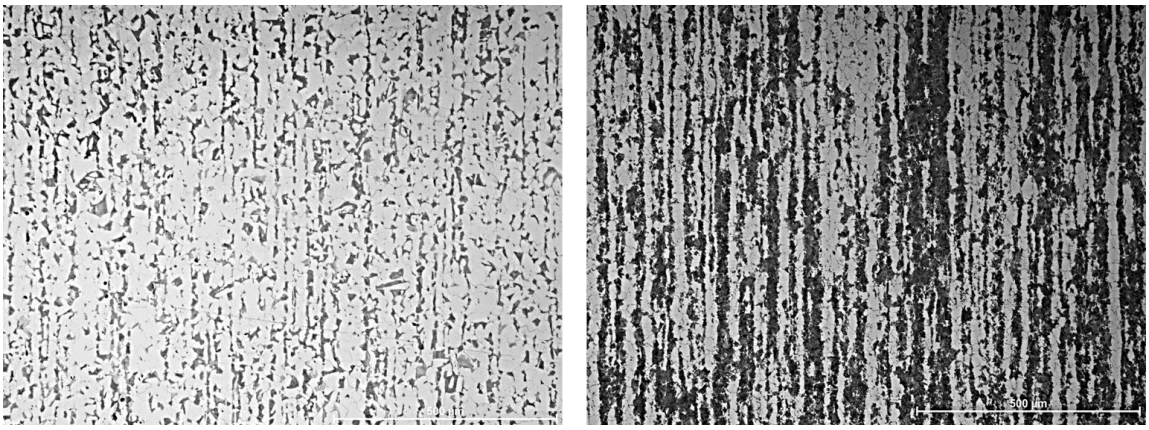

a) b)

Figure 7. Microstructure of the reference samples: a) AISI 1020; b) AISI 4130

A micrography of the laser-hardened samples is shown on the Fig. 8. A partially transformed zone and martensite phase can be observed on the surface of the AISI 1020 sample (Fig. 8 (a)), while laser hardening of the AISI 4130 resulted only in solid-sate transformation (Fig. 8 (b)). Since laser parameters were the same during the treatment process, this effect can be explained either by lower AISI 1020 melting point or its higher absorptivity. No grain refinement in both cases was observed. The heat affected zones for both samples had practically the same depth: 250 µm for AISI 1020 and 248 µm for AISI 4130.

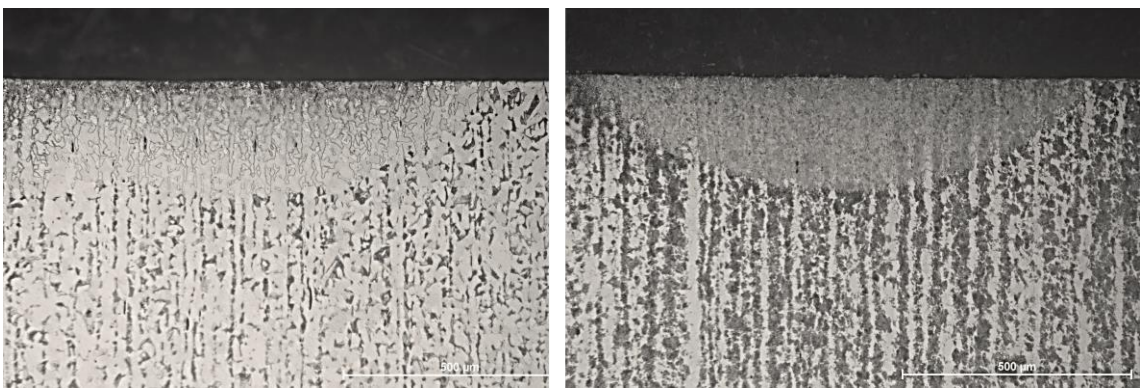

a) b)

Figure 8. Microstructure of the laser-hardened samples: a) AISI 1020; b) AISI 4130

The results of the microhardness measurements for AISI 1020 and AISI 4130 are shown in Figure 9. First of all, it can be observed that the microhardness measured in the reference samples was different for these two materials, demonstrating a mean value of 170±8.8 µm for AISI 1020 and 227±10.5 µm for AISI 4130. This was expected because of the higher amount of perlite in the microstructure of the AISI41XX cast steel group, composed of ferrite and cementite, which is well known for its considerably higher hardness. In addition, the microhardness results were fairly constant (less than 5% of variation for both materials) over the measurement distance. Some variations can be explained by microstructural heterogeneity.

As for the microhardness of the laser-hardened samples, a considerable rise was observed for both materials, reaching 87% for the AISI 1020 specimen and 61% for the AISI 4130 specimen in the near-surface area. The microhardness values decreased as the measurement distance from the surface increased, following the heat affected zone and thermal gradient induced by laser surface processing. Similar tendencies were previously reported by Pakiela et al. (2020) and Furlani et al. (2022). Thus, Catalán et al. (2022) carried out a review on superficial laser heat treatments in cast steels and reported that the highest hardness values were achieved in near-surface regions, where transformation is more homogeneous. However, the microhardness increase in the AISI 1020 sample was considerably higher when compared to AISI 4130 sample, despite the same process parameters used for hardening. This difference is explained by the martensitic phase present on the AISI 1020 surface, as shown in Fig. 8 (a). Therefore, despite the higher mean microhardness of AISI 4130 material, the laser hardening process resulted in a higher superficial/near-superficial hardness of AISI 1020, which can be more useful for service and wear resistance purposes.

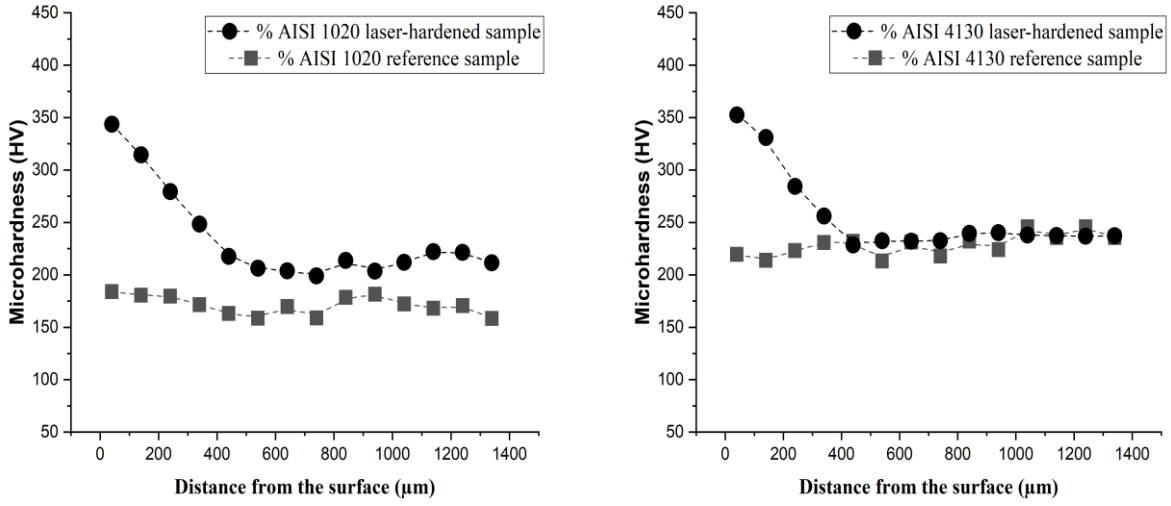

a) b)

Figure 9. Microhardness measured in the reference and laser-hardened samples: a) AISI 1020; b) AISI 4130

Regarding the residual stress measurements induced by the previous manufacturing processes and laser hardening itself, the values in the reference and processed samples can be observed in Figs. 10 and 11 for the longitudinal and transversal components, respectively. Specimens of both materials demonstrated residual stress presence before the heat treatment procedure. For the AISI 1020 case, longitudinal values started at approximately 400 MPa on the surface, decreasing until null values at the 0.3 mm measurement depth. Differently, in the AISI 4130 sample the longitudinal values demonstrated some increase at 0.5-0.1 mm depth at the range of 400 MPa and decreased till negative values (compressive stress) at the depth of 0.25 mm changing therefore not just its magnitude, but also its nature (from tensile to compressive). The transversal component demonstrated the same behavior, except for AISI 4130 there were higher value variations. Similar tendencies have been reported in many previous studies, emphasizing that manufacturing processes such as grinding, cutting, milling, turning etc. imply in local plastic deformation followed by residual stress relocation, as stated by Totten et al. (2002).

As for the residual stress caused by laser hardening in the AISI 1020 sample, it can be observed that for the longitudinal component (Fig. 10(a)), tensile stress was induced by the procedure in the range of 40% (or approximately 170 MPa) when compared with the as-received state. In addition, the residual stress values approached to 0 at a measurement depth of approximately 0.3 mm which is compatible with the heat affected zone size observed in Fig. 8(a). Moreover, a slight increase in the first point of measurement (near-surface residual stress) can be related to the presence of martensite on the laser-processed surface (see Fig. 8(a)).

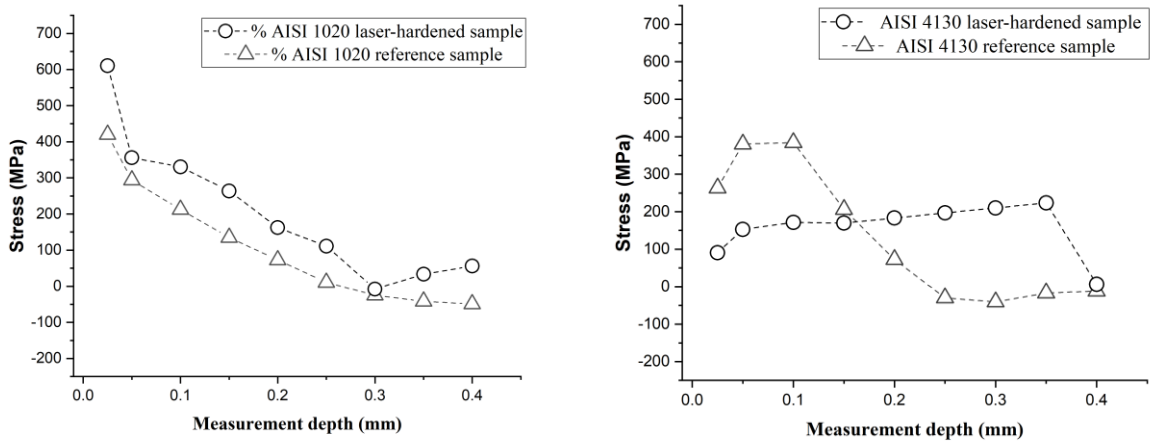

a) b)

Figure 10. Longitudinal stress component in the as-received condition (triangle symbols) and longitudinal residual stress after laser hardening (circle symbols): a) AISI 1020; b) AISI 4130

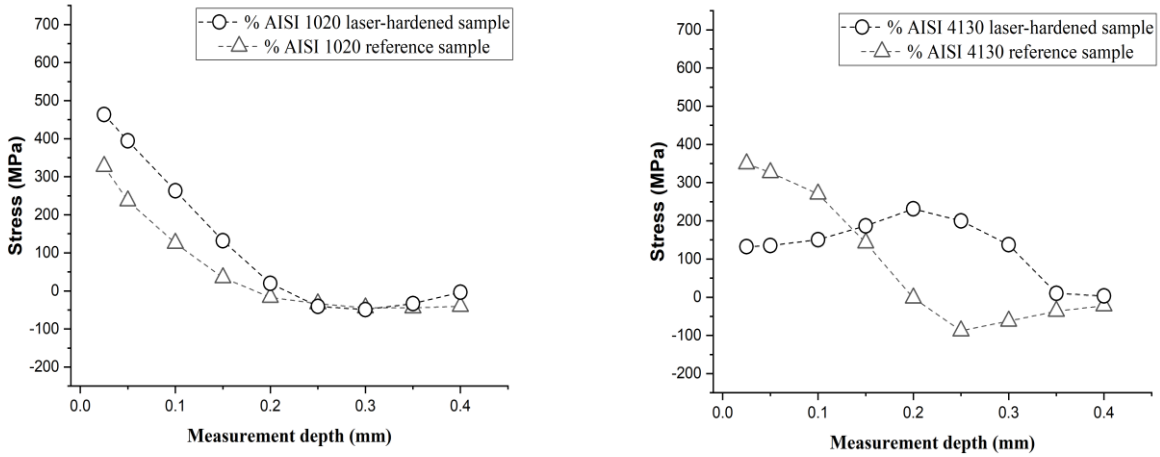

a) b)

Figure 11. Transversal stress component of the as-received condition (triangle symbols) and longitudinal residual stress after laser hardening (circle symbols): a) AISI 1020; b) AISI 4130

On the other hand, compressive residual stress was induced to the AISI 4130 material during the hardening process, despite the exact same process parameters. As can be observed in Fig. 10(b), the tensile stress present originally in the surface and near-surface areas was reduced by approximately 60% (or 200 MPa), fixing the measured values in the range of 100 MPa throughout the measurement distance, suggesting that some kind of stress relief and distribution occurred in the sample during the processing. As reported earlier for the reference as-received samples, the transversal component demonstrated a behavior similar to that of the longitudinal component, both for processed AISI 1020 and AISI 4130 (Figs. 11(a) and 11(b)).

For the reference, compressive residual stress presence in laser hardened AISI 1040 steel was reported previously and discussed by Ganesh et al. (2013) using the same scanner speed applied in this study (10 mm/s), followed by microstructure transformation. However, in this cited study, the compressive (negative) values increased throughout the measurement distance. No information regarding the as-received stress state of the material is provided. In its turn, Kostov et al. (2014) also evidenced compressive stress on the processed surface investigating the multiple pulse effect on residual stress distribution in AISI 4140 during laser hardening. According to Dahotre (1998), this effect can be caused by grid retraction during solid-state transformation in laser processed materials.

Considering the results observed in the present study and those reported earlier in the academic literature, it could be suggested that the nature of the residual stress induced by laser hardening in steels is closely related to the occurrence of martensitic transformations. Thus, when a martensitic transformation takes place on the surface and near-surface area of the processed material, the resulting residual stress tends to be tensile in nature due to the rapid cooling and volumetric expansion experienced by the material. On the other hand, if martensitic transformation occurs in the solid state, the residual stress induced by laser hardening becomes compressive. Gradual transformation and solid-state reorganization during cooling allow for the redistribution of thermal stresses, resulting in a compressive stress state within the material. Future studies for better understanding of the relationship between the occurrence of martensitic transformations and the nature of residual stress are crucial for optimizing the laser hardening process and predicting the mechanical behavior of laser hardened materials.

4. CONCLUSIONS

By comprehensively analyzing the stress profiles in AISI 1020 and AISI 4130 steels before and after laser surface hardening, this study contributes to the existing body of knowledge on residual stress in laser hardened steels. The results reported in this paper show that the materials exhibit different performances when subjected to laser hardening treatment, what should be considered for design, service and wear resistance purposes. Thus, both materials showed martensite formation in the surface area, but only the AISI 4130 steel sample presented compressive stress induced during the hardening process. Meanwhile, tensile stress induction was observed in the AISI 1020 steel sample throughout the analyzed depth. The same effect was reported for both longitudinal and transversal components. Regarding the microhardness results, the AISI 1020 steel showed an increase of almost 87% when superficially hardened, while the AISI 4130 steel presented only an increase of approximately 61%. Therefore, in accordance with the obtained data, it was possible to conclude that, despite of the same process parameters during the treatment, the AISI 4130 steel presents a more effective application of laser surface hardening when compared to the AISI 1020 sample. These differences in stress and hardness may have implications for the performance and service life of laser hardened components made from these materials.

5. ACKNOWLEDGEMENTS

The authors of this study would like to thank to LABENDEM of the Center of Research, Innovation and Development of the state of Espirito Santo, to the Laboratory of Metrology and TRICORMAT of the Federal University of Espirito Santo and to the FINEP founding project for the provided infrastructure and possibility of accomplishment of this study.

6. REFERENCES

Ahmad, M., et al., 2021. “Residual stress analysis of laser-hardened AISI 4140 steel using deep-hole drilling method”, *Journal of Materials Engineering and Performance*, Vol. 30 (2), pp. 1326-1336.

ASTM, American Society for Testing of Materials, 2000. G39-99, *Standard practice for preparation and use of bent-beam stress-corrosion test specimens.*

Barile C., Casavola G., Pappalettere G., Pappalettere C., 2014. “Analysis of the effects of process parameters in residual stress measurements on Titanium plates by HDM/ESPI”, *Measurement*, Vol. 48, pp. 220-227.

Catalán, N., Ramos – Moore, E., Boccardo, A., Celentano, D., 2022. “Surface Laser Treatment of Cast Irons: A Review”. *Metals*, v. 12, n. 4.

Dahotre, N., 1998. “Lasers in Surface Engineering”. *ASM International* (Sudarshan, T. S. Series). ISBN 9781615032235.

Furlani, M. R., Carvalho, S. M., Siqueira, R. H. M., Lima, M. S. F., 2022. “Reduced Coefficient of Friction of Laser Surface Hardened AISI 4130 Steel Substrates”. *Material Design & Processing Communications*, p. 1–9.

Ganesh, P., Kumar H., Kaul, R., Kukreja, L. M., 2013. “Microstructural characterization of laser surface treated AISI 1040 steel with portable X-ray stress analyzer”. *Surface Engineering*, v. 29, n. 8, p. 600–607.

Gao, Y., et al., 2017. “Residual stress and mechanical properties of laser hardened AISI 4340 steel”. *Surface and Coatings Technology*, vol. 324, pp. 648-655.

Huang, S., et al., 2015. “Influence of laser hardening on residual stress and mechanical properties of 30CrMnSiA steel”. *Optics and Laser Technology*, vol. 70, pp. 49-57.

Kostov, V., Gibmeier, J., Lichtenberg, K., Wanner, A., 2014. “Effect of preloading on local residual stresses induced by laser surface hardening of steel”. *Advanced Materials Research*, v. 996, p. 562–567, ISSN 16628985.

Liskevych, O., Almeida, E. M., Feijo, G. F., Macêdo, M. C. S., 2022. “Estudo de aplicabilidade da técnica ESPI (Electronic Specle Pattern Interferometry) combinada com o método do furo-cego para medição de tensões residuais em juntas soldadas”. *Proceedings of the XI Congresso Nacional de Engenharia Mecânica, CONEM 2022,* Teresina – PE, Brasil [in Portuguese].

Lu, J., 1996. *Handbook on measurement of residual stresses*. SEM - Society for Experimental Mechanics, The Fairmont Press, Lilburn, GA, USA.

Marimuthu, S., et al., 2017. “Investigation on the effect of laser hardening on the residual stress distribution in AISI 304 stainless steel”. *Journal of Materials Engineering and Performance*, vol. 26(9), pp. 4290-4302.

Pakieła, W., Tanski T., Brytan, Z., Chladek, G., Pakieła K., 2020. “The impact of laser surface treatment on the microstructure, wear resistance and hardness of the AlMg5 aluminum alloy”. *Applied Physics A: Materials Science and Processing*, Springer Berlin Heidelberg, v. 126, n. 3, p. 1–10, ISSN 14320630.

Steinzig M., Ponslet E., 2003. “Residual stress measurements using the hole drilling method and laser speckle interferometry - Part II: Analysis technique”. *Experimental Techniques*, Vol. 27(4), pp. 17–21.

Sun, J., et al., 2016. “Effects of laser power and scanning speed on residual stress and mechanical properties of selective laser melted 316L stainless steel”, *Journal of Materials Processing Technology*, vol. 238, pp. 218-225.

Totten, G., Howes, M., Inoue, T., 2002. *Handbook of Residual Stress and Deformation of Steel*. ASM International, ISBN 9780871707291.

Upshaw D., Steinzig M., Rasty J., 2011. “Influence of Drilling Parameters on the Accuracy of Hole-drilling Residual Stress Measurements”, Experimental Mechanics, vol. 54(9), pp. 1537-1543.

7. RESPONSIBILITY NOTICE

The authors are the only responsible for the printed material included in this paper.